Room-Temperature Healing of a Thermosetting Polymer Using the Diels–Alder Reaction

Amy M. Peterson,[†] Robert E. Jensen,[‡] and Giuseppe R. Palmese*[,†]

Department of Chemical & Biological Engineering, Drexel University, Philadelphia, Pennsylvania 19104, and U.S. Army Research Laboratory, Aberdeen Proving Ground, Maryland 21005

ABSTRACT Self-healing materials are particularly desirable for load-bearing applications because they offer the potential for increased safety and material lifetimes. A furan-functionalized polymer network was designed that can heal via covalent bonding across the crack surface with the use of a healing agent consisting of a bismaleimide in solution. Average healing efficiencies of approximately 70% were observed. The healing ability of fiber-reinforced composite specimens was investigated with flexural, short beam shear, and double cantilever beam specimens. It was found that solvent amount and maleimide concentration play key roles in determining healing efficiency.

KEYWORDS: biomimetic • Diels–Alder polymers • functionalization of polymers • stimuli-sensitive polymers

INTRODUCTION

Synthetic materials with the ability to heal represent an exciting new field of research. Because they offer potential increased safety and durability, remendable materials are particularly desirable for load-bearing applications in which material failure is costly and a safety concern (1–3). Healing methodologies for polymer networks have focused on two approaches. In one method, polymer networks are made to self-heal by incorporating microcapsules filled with uncured resin as a secondary phase (2, 4–8). Upon fracture, the microcapsules rupture and release resin, which polymerizes to heal the crack. Often, a catalyst is also included within the polymer network to initiate polymerization. The other method relies on the inherent reversibility of bonds designed in a polymer network (9–16). The reversible nature of these linkages allows for network remodeling at the damage site.

Previously reported self-healing chemistries have a number of limitations. Healing mechanisms relying on the polymerization of a secondary phase thermosetting healing agent are restricted in operating temperature by the relationship between the glass transition temperature (T_g) and the cure temperature (T_c). When a thermosetting network cures and vitrifies at a temperature $T = T_c$, it will have a glass transition temperature $T_g \approx T_c$ (17). At any operating temperature $T > T_c$ the polymer network in the healed area will exceed T_g and enter a rubbery state and strength will be compromised. When healing is the result of reversible bonds within the polymer network, mechanical and physical properties are detrimentally affected by an increase in temperature as the equilibrium behavior of the reversible bonds is expressed.

The approach to self-healing composites presented herein improves upon current chemistries. By functionalizing an epoxy-amine network and selecting a reactive healing agent, a healing system was developed in which the healing agent covalently bonds across the crack surface. A solvent is used to deliver the covalent bonding agent and to lower viscosity. The low viscosity of the healing system aids in delivery of the healing agent to cracks, whereas the combination of covalent and physical bonds results in improved load recovery. Work on solvent-based healing systems has appeared in the literature (5, 18) in which incomplete cure of the material being healed is used to achieve healing as diffusion limitations are lowered in the presence of a solvent.

In this work, we report on the furan functionalization of an epoxy-amine thermoset with a tunable T_g as well as the crack healing of this fully cured thermoset using a bismaleimide solution at room temperature under minimal pressure. Healing of the furan-functionalized epoxy-amine thermoset was found to occur multiple times in a given location with healing efficiencies greater than 100% in some cases. Healing of glass fiber-reinforced composites was also investigated with three-point bend, short beam shear, and double cantilever beam specimens.

Load recovery is proposed to be the result of both physical and chemical bonding across the crack surface. Physical bonding is caused by solvent-mediated swelling and interlocking, whereas chemical bonding results from the thermoreversible Diels–Alder reaction of furans and maleimides. This reaction forms a ring structure below 60 °C and reforms the respective diene (furan) and dienophile (maleimide) above 90 °C, which is shown in Figure 1 (19–21). The thermoreversible nature of the Diels–Alder reaction has

* Corresponding author. E-mail: palmese@coe.drexel.edu.
Received for review December 31, 2009 and accepted March 2, 2010
[†] Drexel University.
[‡] U.S. Army Research Laboratory.
DOI: 10.1021/am9009378

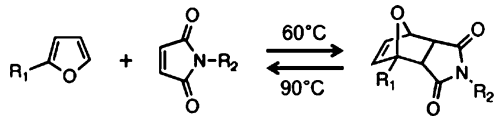

FIGURE 1. Diels–Alder reaction of a furan (left) and a maleimide (right). Below 60 °C, the reactants will form an adduct. At higher temperatures, Diels–Alder adducts will break apart to reform furans and maleimides.

been previously demonstrated at these temperatures with NMR and FTIR, among other characterization methods (20, 22, 23). Healing that relies on this combined mechanism is controlled by diffusion (of both reactant and solvent) as well as reaction. By adjusting the rates of diffusion to match the reaction rate, healing efficiency can be optimized.

EXPERIMENTAL SECTION

Materials. Monomers diglycidyl ether of bisphenol A (DGEBA with EEW=185–192, EPON 828, Miller-Stephenson), furfuryl glycidyl ether (FGE, Sigma-Aldrich), phenyl glycidyl ether (PGE, Sigma-Aldrich), and 4,4′-methylene biscyclohexanamine (PACM, Air Products) were used as received. The healing agent was a solution of 1,1′-(methylenedi-4,1-phenylene)bismaleimide (BMI, Sigma-Aldrich) in *N*,*N*′-dimethylformamide (DMF, Sigma-Aldrich). Chemical structures are shown in Figure 2. Swelling studies of the thermosets were performed in DMF.

Sample Preparation. Furan-functionalized polymers were prepared by adjusting the weight ratio of DGEBA to FGE and mixing these epoxy monomers with a stoichiometric quantity of the amine curing agent PACM. In the discussions that follow, in order to define the polymer networks being considered, $w_{monomer}$ represents the weight fraction of the epoxy monomer in the mixture of monomers bearing the epoxy group (i.e., not including the amine curing agent). For example, a sample containg a 6:4 weight ratio of DGEBA to FGE would have $w_{FGE} = 0.4$ and $w_{DGEBA} = 0.6$. Stoichiometry calculations were carried out using EEW = 188 for EPON 828, 154 for FGE, and AHEW = 52.5 for PACM. For example, a 13.04 g sample of a thermoset with $w_{FGE} = 0.4$ would be prepared by mixing 6.00 g of DGEBA, 4.00 g of FGE, and (6.00/188 + 4.00/154)52.5 = 3.04 g of PACM. Note that for reasons presented in the discussion, most healing studies were conducted with polymers of this composition.

Neat polymer samples were cast and cured for an appropriate amount of time to ensure full reaction, which was validated with differential scanning calorimetry (DSC). For example, samples containing a 10:0 weight ratio of DGEBA to FGE were cured at 80 °C for 2 h and postcured at 165 °C for 2 h (24), whereas samples with a 6:4 weight ratio were cured at 60 °C for 2 h and postcured at 90 °C for 2 h. Control polymers for healing studies were synthesized using PGE instead of FGE. Polymers were prepared with varying weight ratios of DGEBA to PGE and cured using a stoichiometric amount of PACM for an appropriate period of time to ensure complete cure. The EEW of PGE is 164, so to prepare a 13.43 g DGEBA-PGE-PACM specimen with the same cross-link density as a DGEBA-FGE-PACM specimen with $w_{FGE} = 0.4$, 6.00 g of DGEBA, 4.26 g of PGE, and (6.00/188 + 4.26/164)52.5 = 3.04 g of PACM are mixed. This control polymer has an identical cross-link density and network structure to the furan-functionalized network without the furan functionality. Although the control polymer described above has $w_{FGE} = 0.39$, for simplicity it will be described as $w_{FGE} = 0.4$. The $w_{FGE} = 0.4$ polymer was used for most control studies.

Resin transfer molding (RTM) was used to prepare composite specimens with fiber volume fraction ≈24%. The fully mixed resin ($w_{FGE} = 0.4$) was injected into an aluminum mold containing 14 layers of woven glass fibers. The fiber mats were 305 g m^{-2} E-glass fabric from Fiber Glast Developments Corporation, style 7781. Following injection, composites were cured for 2 h at 60 °C and postcured for 2 h at 90 °C.

Swelling Study. The ability of polymer networks to swell in DMF was evaluated by placing fully cured specimens with varying DGEBA:FGE ratios weighing approximately 1.5 g in individual vials and filling each vial with 10 mL DMF. Long-term swelling studies were performed over 35 days at room temperature (22–23 °C). Swelling was measured by removing a polymer specimen from its DMF environment and weighing it at regular intervals. Swelling is defined as mass uptake according to eq 1

$$S = \frac{M_t}{M_0} \times 100\% \quad (1)$$

M_t is the mass uptake of DMF and M_0 is the initial mass of polymer specimens. For specimens that physically degraded as a result of swelling, an attempt was made to recover all pieces of the polymer specimen. However, some error was introduced as a result of such degradation.

Dynamic Mechanical Analysis. Dynamic mechanical analysis was performed with a TA Instruments DMA. T_gs were determined for various polymer formulations at a ramp rate of 2 °C min^{-1} at a frequency of 1 Hz and an amplitude of 15 μm using the dual cantilever geometry. T_g for this study was defined as the inflection point in the storage modulus curve. Specimens were prepared by polishing to the following dimensions: 35 mm × 12.77 mm × 3.15 mm.

Differential Scanning Calorimetry. Differential scanning calorimetry was performed with a TA Instruments DSC Q2000. A ramp rate of 10 °C min^{-1} was selected for scans.

Compact Tension. CT specimen preparation was modified from ASTM D 5045-99 (25) with the introduction of a crack-arresting hole 3.5 mm from the notched end (10, 26). All mechanical testing was performed on an Instron 8872. Figure 3 includes a schematic of the modified CT specimens as well as the testing procedure. The main advantage to the modified compact tension specimen is the crack-arresting hole, which allows for improved crack realignment during healing. A precrack was formed at the base of the notch by lightly tapping with a sharp razor blade. Once CT specimens were fractured, the crack was filled with 10 μL of healing agent using a microsyringe and left to heal at room temperature under minimal pressure for 12 h. This healing time was selected based on kinetic studies of a previous furan-maleimide system (20). After healing, specimens were loaded to failure to determine load recovery for heal 1. Healing efficiency (η_n) for compact tension specimens is defined as

$$\eta_n = \frac{P_n}{P_0} \times 100\% \quad (2)$$

P_n is the maximum load for heal n and P_0 is the maximum load for the initial failure of the specimen. The tests comprising ASTM D 5045–99 are designed to characterize toughness in terms of K_{Ic}, the critical stress intensity factor, and G_{Ic}, the critical strain energy release rate. As it pertains to the specimens used, the relationship between load and displacement is linear with an abrupt drop in the load upon failure. Therefore, G_{Ic} scales with crack length, so maximum load is proportional to G_{Ic}.

Unless otherwise noted, for subsequent healing cycles, specimens were heated at 90 °C for 1 h under no pressure and healed for 12 h at room temperature under minimal pressure. This testing procedure was repeated until specimens no longer recovered load following healing. Minimal pressure (~4.7 kPa) during healing was provided by placing a 240 g plate on top of specimens.

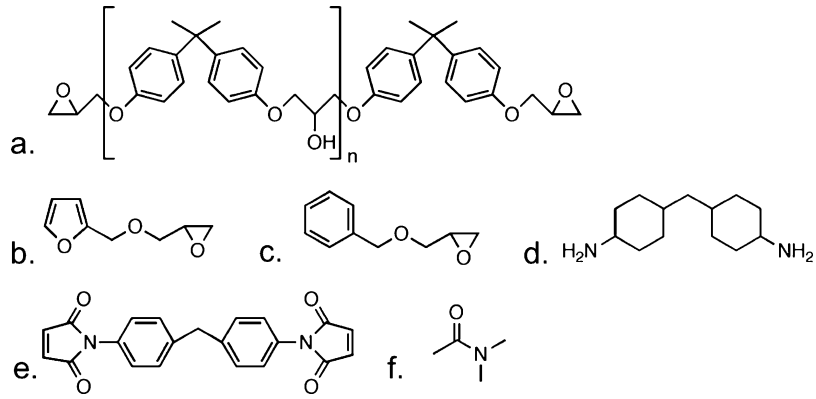

FIGURE 2. Chemical structures of the monomers used for the preparation of healable networks. (a) DGEBA, $n = 0.13$, (b) FGE, (c) PGE, (d) PACM; and chemical structures of the healing agent (e) BMI, (f) DMF. The amine cured epoxy network is furan functionalized using the monofunctional FGE monomer. Analogous networks replacing furan functionality with pendant phenyl groups are prepared using PGE. The healing agent is a solution of BMI in DMF.

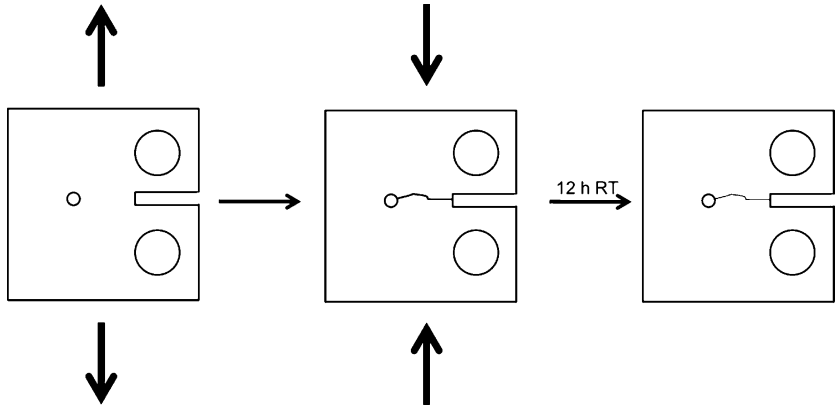

FIGURE 3. Schematic of CT specimen failure and healing. The virgin specimen is loaded in tension until a crack forms. Healing agent is injected into the crack and the specimen is allowed to heal for 12 h at ambient conditions (~22 °C).

Flexural Strength. Glass fiber-reinforced composite rectangular specimens with dimensions 125 mm × 12.5 mm × 6.35 mm were tested in accordance with ASTM D 790-03 (27). Specimens were loaded to failure in flexure at a rate of crosshead motion $R = 2.71$ mm min^{-1} with a 16:1 span to thickness ratio. This large ratio results in tensile failure, emphasizing fiber strength. Following failure, holes were drilled into the failure site and 25−75 μL of healing agent was injected into the specimen. Specimens were then healed at room temperature for one day under pressure. Following healing, specimens were again loaded to failure under the same conditions.

Fiber-reinforced composites retain residual mechanical properties once failed, that is, if a specimen is tested until there is a 40% drop in the stress, subsequent loading will result in a stress−strain curve with the maximum value at 60% of the initial max stress. To evaluate the healing ability of fiber-reinforced composites, we have chosen to compare healed mechanical properties to the mechanical properties of failed but unhealed specimens. Equation 3 describes healing efficiency for three point bend specimens.

$$\eta = \frac{P_{\text{healed}} - P_{\text{unhealed}}}{P_{\text{initial}} - P_{\text{unhealed}}} \times 100\% \qquad (3)$$

Flexural properties are evaluated with the procedures specified in ASTM D 790-03 (27). Typically, flexural stress, σ_f, is reported from ASTM D 790-03 (27). Load is proportional to σ_f.

Short-Beam Strength. Short-beam specimens of glass fiber-reinforced composites were prepared and tested in accordance with ASTM D 2344/D 2344M-00 with the following dimensions: 50 mm × 12.5 mm × 6.35 mm (28). Specimens were tested with a span to thickness ratio of 3:1. To deliver healing agent to the failure site, we included glass capillary tubes in the composite pieces. These capillary tubes were attached to pipettes filled with 50 μL of healing agent. Specimens were loaded to failure in flexure at a rate of 12.5 mm min^{-1}. Upon failure, healing agent was pushed from the pipet into the capillary tube, and subsequently into the failure site. Specimens were healed at room temperature for 1−7 days under pressure, and were then loaded to failure under the same test conditions. Figure 4 shows images of a specimen at different points in the testing procedure. This test method allows for determination of the short-beam strength, F^{sbs} of the material, which is described below and is proportional to the maximum load

$$F^{\text{sbs}} = 0.75\frac{P_m}{bh} \qquad (4)$$

In eq 4, P_m is the maximum load observed during testing and b and h are the specimen width and thickness, respectively. Healing efficiency for short beam shear specimens is therefore determined by the following expression

$$\eta = \frac{P^{\text{sbs}}_{\text{healed}} - P^{\text{sbs}}_{\text{unhealed}}}{P^{\text{sbs}}_{\text{initial}} - P^{\text{sbs}}_{\text{unhealed}}} \times 100\% \qquad (5)$$

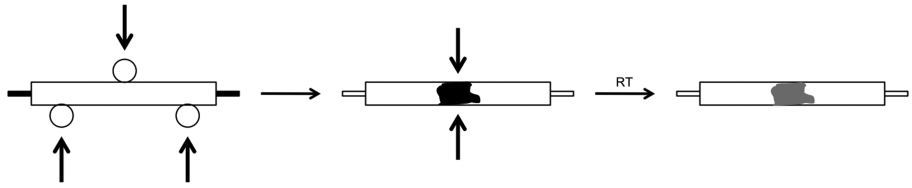

FIGURE 4. Images of short beam specimens testing procedure. The specimen is failed (left), healing agent flows from the fiber to the failure site (center), allowing for the specimen to heal (right).

Typical failure modes for short beam shear specimens include interlaminar shear, flexure (compression or tension), and inelastic deformation.

Double Cantilever Beam. Double cantilever beam (DCB) specimens of glass fiber-reinforced composites with dimensions 125 mm × 25 mm × 6.35 mm were prepared and tested in accordance with ASTM D5528−01 (29). Specimens were loaded in tension at a rate of 2 mm min^{-1} to form a precrack, were unloaded, and then were subsequently reloaded at the same rate to a crack length of 40 mm. While still loaded at a crack length of 40 mm, 0.5 g (53 μL) of healing agent was injected into the interface between specimen sides. Specimens were healed at room temperature for seven days under pressure. Following healing, specimens were loaded to a crack length of 40 mm at a rate of 2 mm min^{-1}. This procedure allows for calculation of the interlaminar fracture toughness G_{Ic}.

$$G_{Ic} = \frac{3P\delta}{2ba} \tag{6}$$

In eq 6, P is load, δ is the load point displacement, and a is the delamination length. Healing efficiency for double cantilever beam specimens is defined as

$$\eta = \frac{G_{Ic,healed} - G_{Ic,unhealed}}{G_{Ic,initial} - G_{Ic,unhealed}} \times 100\,\% \tag{7}$$

With this testing procedure, G_{Ic} increases initially, but stabilizes with delamination growth. The G_{Ic} values in eq 6 are therefore the stabilized value for each system.

RESULTS AND DISCUSSION

Swelling Study. Since the healing agent for this self-healing system is a DMF-based solution, swelling in DMF is an important consideration. The results of the equilibrium swelling study are given in Figure 5. As described in the sample preparation section, the composition of the networks being evaluated is specified by the weight fraction of FGE or PGE based on the total weight of epoxide-bearing monomers. Swelling increases with relative amount of FGE, which is consistent with expected changes in network structure. FGE has an epoxy functionality $f = 1$, so increased FGE content decreases cross-linking, which allows for greater swelling of the network. Additionally, the swelling behavior was evaluated for networks where PGE was substituted for FGE at an equivalent $w_{monomer}$ to study the effect of furans within the polymer network when compared to that of pendant phenyl groups. The DGEBA-FGE-PACM system with $w_{FGE} = 0.4$ and the DGEBA-PGE-PACM system with $w_{PGE} = 0.4$ are analogous. The equilibrium mass uptake reaches values in excess of 100% for the more lightly cross-linked

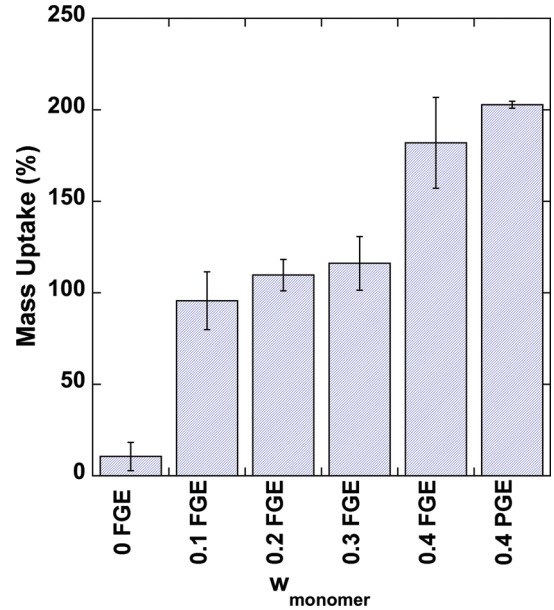

FIGURE 5. Swelling (mass uptake) of thermoset systems in DMF. These values represent equilibrium mass uptake values. The cross-link density of a network with $w_{FGE} = 0.4$, $w_{DGEBA} = 0.6$, and a stoichiometric amount of the PACM cross-linking agent is practically the same as a thermoset with $w_{PGE} = 0.4$, $w_{DGEBA} = 0.6$, and a stoichiometric amount of PACM.

systems. Moreover, the swelling behavior is very similar for the analogous furan- and phenyl-functionalized networks described above, suggesting that changes in cross-link density are primarily responsible for equilibrium swelling behavior for the materials selected.

Thermomechanical Polymer Characterization. T_gs were determined for various polymer formulations via differential scanning calorimetry and corroborated using dynamic mechanical analysis. Figure 6 shows the relationship between T_g and loading of FGE. The Fox Equation, which describes the T_g of a multicomponent polymer as a function of relative amounts, was used to fit the experimental T_g data (30)

$$T_g = \frac{w_a}{T_{g,a}} + \frac{w_b}{T_{g,b}} \tag{8}$$

In the case of the DGEBA-FGE-PACM system, w_a is the weight fraction of DGEBA and w_b is the weight fraction of FGE as compared to the total weight of epoxide-bearing monomers (DGEBA and FGE). $T_{g,a}$ corresponds to the T_g of a system containing a stoichiometric mixture of DGEBA and PACM, whereas $T_{g,b}$ corresponds to the T_g of a system containing a stoichiometric mixture of FGE and PACM. The Fox Equation

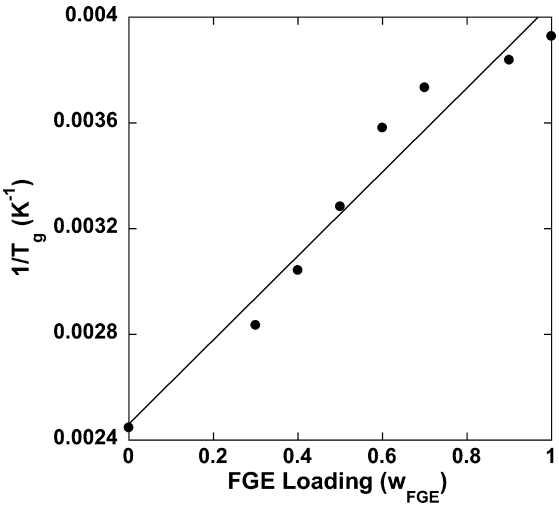

FIGURE 6. Relationship between T_g and FGE content. The decrease in T_g with increasing FGE content is in good agreement with the Fox equation.

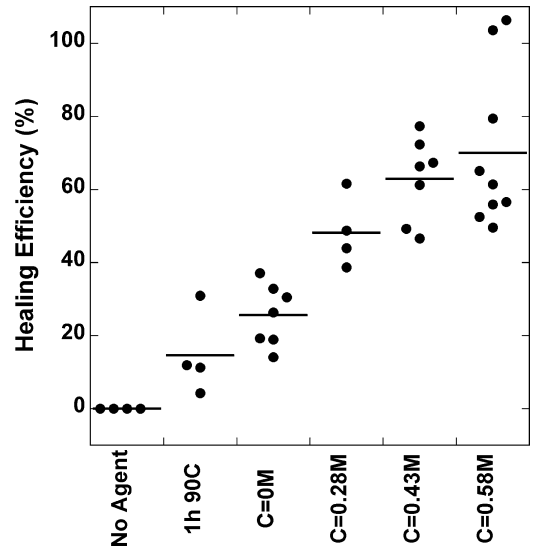

FIGURE 7. Healing efficiency of furan-functionalized CT specimens with various healing agents, first heal. Healing agents were solutions of BMI in DMF, concentration refers to the concentration of BMI. Each dot represents a single data point, bars represent average healing efficiency for the data set.

assumes uniform morphology; therefore, the good agreement ($R^2 = 0.956$) with the DGEBA-FGE-PACM systems implies that the networks are relatively homogeneous. Indeed, no visible signs of phase separation were apparent as all of the samples studied were optically transparent.

The network with $w_{FGE} = 0.4$ was chosen for further characterization and as the polymer network for self-healing studies. This network in particular was selected for its low T_g (55.6 °C) and high amount of swelling in the healing agent solvent. Both factors were assumed necessary to maximize the Diels–Alder bonding across a crack surface. This polymer was found to have fracture toughness $G_{Ic} = 920$ J m^{-2}, tangent modulus of elasticity $E_B = 3.3$ GPa, and flexural strength $\sigma = 73$ MPa. Dynamic mechanical analysis of the material over a range of temperatures and frequencies showed a single alpha relaxation with activation energy $E_a = 393$ kJ mol^{-1}, corresponding to the glass transition of the material and further indicating material homogeneity. On the basis of the plateau loss modulus obtained by DMA, a molecular weight between cross-links (M_c) of 4.4 kg mol^{-1} was found. DSC corroborated the DMA-determined T_g with a value of 58.6 °C.

Polymer Healing. The ability of DMF-based BMI solutions to function as healing agents was evaluated by measuring crack healing of failed CT specimens via direct application of the healing agent to the crack surface. The ability to recover load-bearing capacity using BMI solutions of different concentrations was measured and compared to that of pure DMF as well as heating CT specimens above their T_g at 90 °C for 1 h. Figure 7 shows healing efficiencies for the first heal using different healing agents as compared to the load at failure of the virgin system. Each set of points represents data for a given healing condition and the horizontal line marks the average healing efficiency for the set of points. An average healing efficiency of 28.4 ± 8.3% was observed when pure DMF ($C = 0$ M) was used as healing agent and 14.6 ± 11.4% for dry healing above T_g (1 h, 90 °C). Healing efficiency increased greatly with increasing BMI concentration up to 0.58 M. The use of BMI healing agent solution with a maleimide concentration of 0.58 M resulted in an average healing efficiency of 70.0 ± 21.6%, with two data points demonstrating healing greater than 100%. Healing efficiency was dependent upon how effectively the healing agent was injected into the crack. It is important to note that the healing efficiency of some specimens indicate healed strength higher than the initial strength of the virgin specimen. These results show the true potential healing capacity of this system. It was found that incomplete coverage of the crack surface with healing agent resulted in lower healing efficiency. Filling the crack was difficult, in part because of the polymer network's affinity for swelling in DMF. As shown in Figure 7, load recovery increased with increasing BMI concentration, suggesting that covalent bonding is an important mechanism for strength recovery. However, healing is possible for systems containing no BMI; therefore, healing is not solely the result of covalent bonding across the crack surface.

The capacity to heal multiple times was investigated for the 0.58 M BMI solution, pure DMF, and 1 h at 90 °C dry treatment. For healing cycles past the first, these specimens were heated at 90 °C for 1 h to break apart Diels–Alder adducts and soften the polymer network, followed by healing at room temperature under minimal pressure for 12 h when presumably Diels–Alder adducts would have the opportunity to reform. Results of these experiments are shown in Figure 8. Specimens healed with 0.58 M BMI recovered 70.0 ± 21.6% and 73.5 ± 7.7% of initial strength for the first two heals, respectively. Following the third healing cycle, load recovery dropped off significantly and was in the same range as load recovery for the two other healing agents. This decrease in healing efficiency could be the result of diffusion of BMI molecules away from the crack surface or physical degradation of the crack surfaces as a result of multiple failure cycles. The abrupt drop indicates that diffusion is more likely.

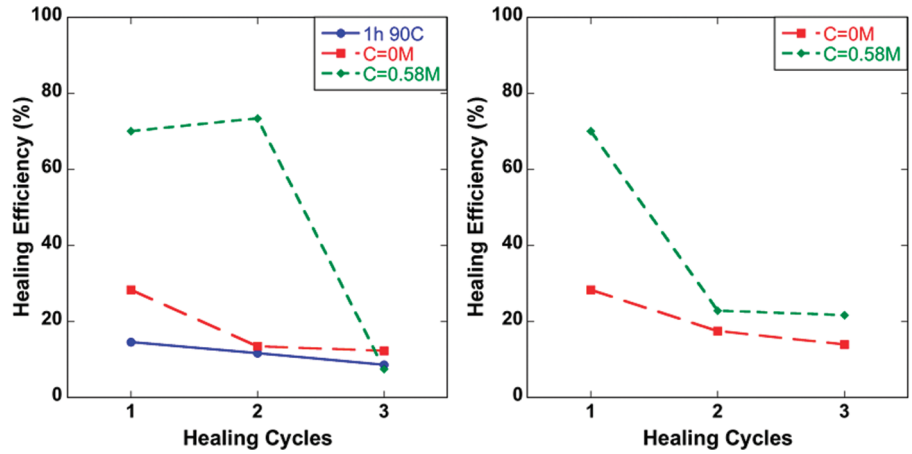

FIGURE 8. Healing efficiency results for multiple healing cycles of furan-functionalized CT specimens. Two methods were investigated for second and third heals: 90 °C for 1 h, room temperature for 12 h (left) or 10 μL DMF, room temperature for 12 h (right). Labels describe first heal conditions. Healing agent were solutions of BMI in DMF.

Additional healing studies were performed in which the reheal procedure was modified. Instead of heating at 90 °C for 1 h, 10 μL of DMF was injected in the crack surface for each healing cycle past the first. Specimens were then allowed to heal at ambient conditions under minimal pressure for 12 h. Results are shown in Figure 8. In the case of healing with the 0.58 M BMI solution, adding DMF resulted in significantly lower healing efficiency than healing using the dry heat procedure (22.9 ± 9.7% vs 73.5 ± 7.7%). Such behavior indicates that perhaps additional DMF increases BMI mobility and allows for its diffusion away from the crack surface, whereas heating and cooling allow for the breakage and reformation of bonds across the fracture surface. Nevertheless, when 0.58 M BMI is used for the first healing cycle, healing efficiencies after multiple healing cycles remain higher than when DMF is used for the first healing cycle. After three healing cycles the 0.58 M BMI-healed system still recovered 21.7 ± 2.2% of the initial strength, but the DMF-healed system dropped to 14 ± 2.4% of strength recovered. When specimens were healed with DMF repeatedly (five cycles) healing efficiencies of 0% was found for all specimens tested, whereas some specimens healed initially with 0.28 or 0.58 M BMI solution showed significant strength recovery even after six healing cycles. Those specimens recovered 16.0 and 23.1% of their initial strength, respectively.

Healing of analogous furan-free polymer networks was also investigated. This was done to further evaluate the role of covalent bonding on healing. The results of these experiments are shown in Figure 9. Healing of a DGEBA−PACM network ($w_{FGE} = 0$) resulted in 0% healing efficiency for all healing agents. Given that healing was observed for maleimide-free healing systems in a lower T_g DGEBA-FGE-PACM network ($w_{FGE} = 0.4$), this inability to heal results from a high cross-link density, high T_g, and corresponding low swelling in DMF. A furan-free polymer network with the same cross-link density as the DGEBA−FGE−PACM network with $w_{FGE} = 0.4$ was prepared using PGE instead of FGE, i.e., DGEBA−PGE−PACM ($w_{PGE} = 0.4$). This polymer had $T_g = 74.4$ °C according to DMA, compared to 55.6 °C for the analogous FGE system. When healed with DMF, a healing efficiency of

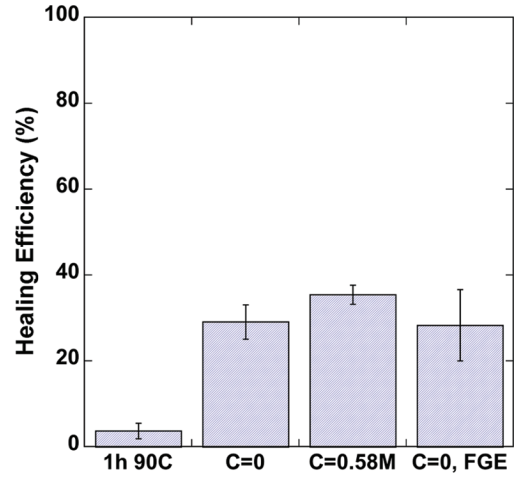

FIGURE 9. Healing efficiency for furan-free networks. This thermoset is a PGE-modified network with the same cross-link density as the furan-functionalized network with $w_{FGE} = 0.4$. For comparison, the healing efficiency of DMF with the furan-functionalized network with $w_{FGE} = 0.4$ is included. Healing agents were solutions of BMI in DMF.

29.1 ± 4.0% was found, as compared to 35.5 ± 2.2% when 0.58 M BMI was used. These values are within error of each other. Furthermore, they are close to the 28.4% healing efficiency obtained for the DGEBA−FGE−PACM ($w_{FGE} = 0.4$) system healed using pure DMF. It is apparent that the addition of BMI does not significantly affect healing efficiency of the furan-free network and it is concluded that covalent bonding plays a prominent role in healing furan-functionalized networks with BMI solutions.

Composite Healing. Healing of fiber-reinforced composites is a complex process. As compared to a neat polymer system, which consists of a single polymer phase, composites have resin and fiber phases as well as the high-stress interface between the two. The self-healing mechanisms thus far reported in the literature have focused on healing of the resin phase (31–34), although Blaiszik et al. have reported methods for healing interfacial failure (6). It is at this time not feasible to heal carbon or glass fiber failure, although autonomous silica formation has been considered for glass fibers (35, 36). Notwithstanding the difficulties

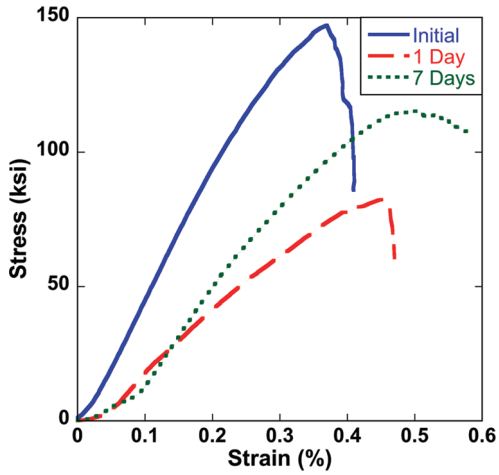

FIGURE 10. Stress–strain curves for healing of a composite specimen following flexural failure. Specimens were healed with 0.15 g of 0.58 M BMI in DMF. The virgin specimen's behavior is solid, a specimen healed for 1 day is shown as a dashed line, and the curve for a specimen healed for 7 days is shown as a dotted line.

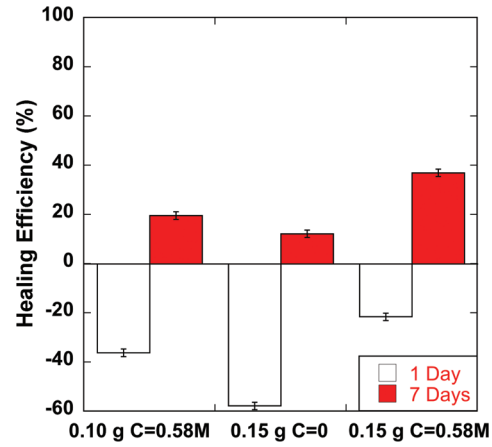

FIGURE 11. Healing efficiencies for short beam shear specimens after failing and healing for 1 or 7 days. Healing agents were solutions of BMI in DMF. Note that healing efficiencies are normalized by the load recovery of unhealed specimens.

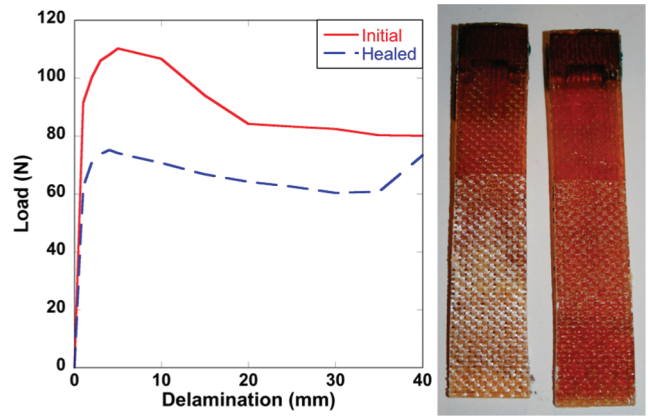

FIGURE 12. Load-delamination behavior for a virgin (solid) and healed (dashed) double cantilever beam specimen is shown on the left. Specimens were healed with 0.5 g of 0.58 M BMI in DMF. Two sides of a specimen following failure are shown on the right. Fibers are clearly exposed on one side of the double cantilever beam specimen.

associated with healing the reinforcing phase of a composite upon failure, it is of value to investigate the degree to which matrix healing provides healing in composites fractured in different ways. Therefore, the healing behavior of glass fiber/DGEBA–FGE–PACM systems failed in flexure, in short-beam shear, and in mode I interlaminar fracture have been investigated.

Three point bend specimens were used to evaluate the ability to heal flexural failure. Specimens were healed with 0.15 g of 0.58 M BMI solution in DMF by direct injection of healing agent into the failure site as described in the procedure section. Representative stress–strain results for three point bend healing are shown in Figure 10. Healing for 1 day resulted in a negative healing efficiency (−5.7%) as defined by eq 3, whereas healing for 7 days gave a healing efficiency of 47.9%. Note that healing efficiency is related to the residual strength of the material, not the strength of the virgin composite. The stress–strain curve for 1 day of healing has a much lower slope (modulus) than the initial specimen and the one healed for 7 days. Additionally, the peak in the stress–strain curve for 1 day of healing occurs at almost the same stress and strain values as the final loading point of the initial curve. The large increase in healing efficiency between one and seven days can be attributed to diffusion of solvent out of the composite with consequent recovery of modulus as well as a potential increase in covalent bonds across the crack surface over the additional 6 days.

Short-beam shear specimens were investigated next in an effort to increase the relative occurrence of interlaminar failure and potentially provide a composite failure mode more dependent on matrix healing. In this case, glass tubes containing the healing agent were placed within the composite and allowed to rupture in flexure, thus simplifying healing agent delivery. Figure 11 shows healing efficiency values for a number of healing agent systems. Healing efficiencies as defined by eq 4 increased for all systems from 1 day of healing to 7 days of healing. No specimens demonstrated a positive healing efficiency after 1 day. However, all healing agents resulted in positive healing efficiencies, with up to 37.1% after seven days of healing. Healing efficiencies are greater in all cases when BMI is included in the healing agent solution; 0.15 g of 0.58 M BMI solution has a greater healing efficiency than 0.10 g of 0.58 M BMI solution (19.7 vs 37.1% after 7 days).

The DCB testing configuration was selected to focus as much as possible on failure of the resin phase. Figure 12 displays load vs delamination results for a virgin and healed specimen. 67.6% of interfacial strength was recovered. Evaluation of the surfaces reveals a large number of exposed fibers. Therefore, failure occurs primarily along the resin-fiber interface. Based on optical analysis of the fracture surfaces, one surface consisted of 95.0% resin, while the other consisted of 34.8% resin. This suggests that approximated 30–35% of the interlaminar failure occurred by cohesive failure of the healable polymer. Surface composition mapping using FTIR microscopy showed that areas attributed to polymer via optical analysis showed high absorbance of chemical moieties found in the polymer and

healing agent, such as the absorbance at 1713 cm^{-1} for maleimide C═O symmetric stretching (37). Areas attributed to the bare glass fiber showed strong absorbance at 1062 cm^{-1} associated with silicate Si−O−Si asymmetric bond stretching (38). The average interfacial strength found with the DCB tests was 49.6%. The fact that in all cases a majority of the interlaminar failure was fiber-matrix adhesive failure suggests that healing of the cohesive polymer failure was efficient and complete.

Healing Mechanism. Dependence of healing efficiency on BMI concentration indicates that BMI reacts across the crack surface. The primary healing mechanism is covalent bond formation across the crack surface. At room temperature furans and maleimides react via cycloaddition to form Diels−Alder adducts. In this system, BMI reacts with surface furans. If the distance between fracture surfaces is less than the length of a BMI molecule, bonding can occur across the crack. Between 60 and 90 °C, adducts break apart and reform the original furans and maleimides, which is how the procedure for healing over multiple cycles was chosen.

Strength recovery of the $w_{FGE} = 0.4$ network with a BMI-free healing agent as well as healing of a furan-free network indicates that a secondary mechanism of mechanical interlocking contributes to healing. Mechanical interlocking is related to rubber-like behavior, induced either by swelling of the polymer matrix or of heating the network above its T_g (26). Solvent-mediated swelling and subsequent deswelling results in mechanical interlocking of nodes on opposing fracture surfaces. Increasing the temperature above its T_g is postulated to have a similar softening effect, although the use of DMF has been demonstrated to have a greater softening effect in the investigated networks than increasing the temperature 35 °C above the materials' T_g values. Swelling/softening is necessary to facilitate healing via mechanical interlocking of the fracture surfaces, which is indicated by the inability of the DGEBA-PACM ($w_{FGE} = 0$) to heal under the conditions investigated. This particular thermosetting network has been shown to recover significant strength under more extreme temperatures and pressures (26).

Additionally, swelling brings opposite fracture surfaces into intimate contact with each other, allowing for more covalent bonding across the crack surface. Swelling or softening is necessary because cracks tend to be on the micrometer scale (26), whereas the BMI molecule is approximately 1.3 nm in length. Figure 13 shows how swelling improves the amount of covalent bonding. When the furan-functionalized network is fractured, furan groups are exposed along the crack surface. The BMI-based healing agent then flows into the crack. The solvent diffuses into the polymer, swelling the material and bringing opposing crack surfaces into intimate contact with each other. Simultaneously, maleimides in the BMI react with polymer-bound furans. Where the distance between the crack surfaces is ≤1.3 nm, BMI molecules can react with both sides of the crack, covalently bonding material and bringing opposing crack surfaces into intimate contact with each other, causing

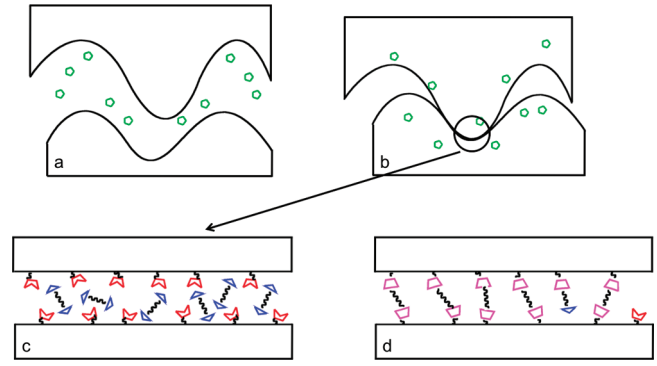

FIGURE 13. Proposed healing mechanism. Green pentagons represent solvent molecules, red notched trapezoids represent furans, blue triangles represent maleimides, and magenta trapezoids represent Diels−Alder adducts. (a) Healing agent is injected in the crack. (b) Solvent swells the polymer network. (c) On the nanoscale, furans along the crack surface come into contact with BMIs. (d) BMIs react with furans and covalently bond across the crack surface.

interlocking of these crack surfaces. While the polymer is swelled, furans along the crack surfaces react with bismaleimides, forming covalent bonds across the crack surface Over time, the solvent evaporates and the polymer deswells, but these physical and covalent bonds remain. The selected polymer network with $f_{FGE} = 0.4$ swells to 200% of its original weight in DMF.

To optimize healing efficiency, the amount of solvent and BMI must be controlled. Too little solvent results in limited swelling and, consequently, little mechanical interlocking and covalent bonding. However, too much solvent can cause physical degradation of the polymer network or an extended time for mechanical properties to be recovered. If there are not enough BMI molecules in the healing agent, few covalent bonds can form across the crack surface. Too many BMI molecules reduce the probability that a single molecule would react twice and bond the crack together. Future work includes performing such optimization.

CONCLUSIONS

A novel self-healing system capable of recovering strength at room temperature has been developed. Healing is the result of physical and covalent bonding. Solvent-induced swelling and softening of the crack surfaces allows for mechanical interlocking, while compatible functionalization of the polymer network and healing agent causes covalent bonding through the Diels−Alder reaction of furans and maleimides. Physical bonding results in 28.4% recovery of the initial strength, whereas covalent bonding results in an additional 41.6% healing efficiency. Average healing efficiencies of 70% were observed, with two specimens recovering >100% of the initial strength.

Incorporation of this healing chemistry in polymer composites was investigated. A new method of defining healing efficiency in polymer composites was proposed. By normalizing for the residual strength of an unhealed composite, this definition more accurately represents the healing ability of the chemistry. For flexure and short-beam shear specimens, significant irreversible fiber damage was observed. An average of 49.6% of interfacial strength was recovered with a

double cantilever beam geometry. However, the specimen failed primarily at the fiber−resin interface, resulting in limited locations for covalent bonding with polymer network across the failure surface.

Future work will focus on developing methods of incorporating BMI solutions in composites. Possibilities include hollow glass fibers and polymer microcapsules. Other polymer networks, such as furan-functionalized polyurethanes and vinyl esters, are being investigated. Additionally, we plan to improve our understanding of the mechanisms of healing for this healing system so as to create materials with improved healing abilities. Topics of interest include quantifying the effects of T_g, solvent, BMI concentration, and BMI structure on healing.

Acknowledgment. The authors wish to acknowledge the U.S. Army Research Laboratory for financial support under the Army Materials Center of Excellence Program, contract W911NF-06-2-0013. Financial support for Amy M. Peterson was provided by the National Science Foundation under the Integrated Graduate Education and Research Traineeship in Nanoscale Science and Engineering administered by Drexel University and the University of Pennsylvania, Contract DGE-0654313, as well as the Graduate Research Fellowship Program. The authors also thank Claude Robotham and Joseph Dorsheimer of Thermo Fisher Scientific for DCB specimen surface analysis.

REFERENCES AND NOTES

(1) Pang, J. W. C.; Bond, I. P. *Composites, Part A* **2005**, *36*, 183–188.
(2) White, S. R.; Sottos, N. R.; Geubelle, P. H.; Moore, J. S.; Kessler, M. R.; Sriram, S. R.; Brown, E. N.; Viswanathan, S. *Nature* **2001**, *409*, 794–797.
(3) Williams, G.; Trask, R.; Bond, I. P. *Composites, Part A* **2007**, *38*, 1525–1532.
(4) Cho, S. H.; Andersson, H. M.; White, S. R.; Sottos, N. R.; V, B. P. *Adv. Mater.* **2006**, *18*, 997–1000.
(5) Caruso, M. M.; Delafuente, D. A.; Ho, V.; Sottos, N. R.; Moore, J.; White, S. R. *Macromol. Rapid Commun.* **2007**, *40*, 8830–8832.
(6) Blaiszik, B. J.; Sottos, N. R.; White, S. R. *Compos. Sci. Technol.* **2008**, *68*, 978–986.
(7) Pang, J. W. C.; Bond, I. P. *Compos. Sci. Technol.* **2005**, *65*, 1791–1799.
(8) Yuan, L.; Liang, G.-Z.; Xie, J.-Q.; Guo, J.; Li, L. *Polym. Degrad. Stab.* **2006**, *91*, 2300–2306.
(9) Chen, X.; Dam, M. A.; Ono, K.; Mal, A.; Shen, H.; Nutt, S. R.; Sheran, K.; Wudl, F. *Science* **2002**, *295*, 1698–1702.
(10) Chen, X.; Wudl, F.; Mal, A. K.; Shen, H.; Nutt, S. R. *Macromolecules* **2003**, *36*, 1802–1807.
(11) Murphy, E. B.; Bolanos, E.; Schaffner-Hamann, C.; Wudl, F.; Nutt, S. R.; Auad, M. L. *Macromolecules* **2008**, *41*, 3169–3174.
(12) Kalista, S. J.; Ward, T. C. *J. R. Soc. Interface* **2007**, *4*, 405–411.
(13) Liu, Y.; Hsieh, C. *J. Polym. Sci., Part A* **2006**, *44*, 905–913.
(14) Liu, Y.; Hsieh, C.; Chen, Y. *Polymer* **2006**, *47*, 2581–2586.
(15) Wolfgang, H. B.; Robert, S. *Macromol. Rapid Commun.* **2007**, *28*, 15–54.
(16) Kavitha, A. A.; Singha, N. K. *J. Polym. Sci., Part A* **2007**, *45*, 4441–4449.
(17) Enns, J.; Gillham, J. *J. Appl. Polym. Sci.* **1983**, *28*, 2567–2591.
(18) Blaiszik, B. J.; Caruso, M. M.; McIlroy, D. A.; Moore, J. S.; White, S. R.; Sottos, N. R. *Polymer* **2009**, *50*, 990–997.
(19) Costanzo, P. J.; Demaree, J. D.; Beyer, F. L. *Langmuir* **2006**, *22*, 10251–10257.
(20) Peterson, A. M.; Jensen, R. E.; Palmese, G. R. *ACS Appl. Mater. Interfaces* **2009**, *1*, 992–995.
(21) Peterson, A. M.; Palmese, G. R. *Reversible Diels−Alder Cycloaddition for the Design of Multifunctional Network Polymers*; Wiley: New York, 2009.
(22) McElhanon, J.; Wheeler, D. *Org. Lett.* **2001**, *3*, 2681–2683.
(23) Kavitha, A.; Singha, N. K. *ACS Appl. Mater. Interfaces* **2009**, *1*, 1427–1436.
(24) Palmese, G. R.; McCullough, R. L. *J. Appl. Polym. Sci.* **1992**, *46*, 1863–1873.
(25) *ASTM D5045-99 Standard Test Methods for Plane-Straine Fracture Toughness and Strain Energy Release Rate of Plastic Materials*; ASTM International: West Conshohocken, PA, 2007; pp 1−9.
(26) Rahmathullah, M. A. M.; Palmese, G. R. *J. Appl. Polym. Sci.* **2009**, *113*, 2191–2201.
(27) *ASTM D790-03 Standard Test Methods for Flexural Properties of Unreinforced and Reinforced Plastics and Electrical Insulation Materials*; ASTM International: West Conshohocken, PA, 2003; pp 1−11.
(28) *ASTM D2344/D2344M-00 Standard Test Method for Short-Beam Strength of Polymer Matrix Composite Materials and Their Laminates*; ASTM International: West Conshohocken, PA, 2000; pp 1−8.
(29) *ASTM D5528-01 Standard Test Method for Mode I Interlaminar Fracture Toughness of Unidirectional Fiber-Reinforced Polymer Matrix Composites*; ASTM International: West Conshohocken, PA, 2001; pp 1−12.
(30) Sheng, X.; Kessler, M.; Lee, J. *J. Therm. Anal. Calorim.* **2007**, *89*, 459–464.
(31) Kessler, M. R.; Sottos, N. R.; White, S. R. *Composites, Part A* **2003**, *34*, 743–753.
(32) Pang, J.; Bond, I. P. *Compos. Sci. Technol.* **2005**, *65*, 1791–1799.
(33) Trask, R.; Williams, G.; Bond, I. P. *J. R. Soc. Interface* **2006**, *4*, 363–371.
(34) Hayes, S. A.; Jones, F. R.; Marshiya, K.; Zhang, W. *Composites, Part A* **2007**, *38*, 1116–1120.
(35) Pogula, S. D.; Patwardhan, S. V.; Perry, C. C.; Gillespie; Yarlagadda, S.; Kiick, K. L. *Langmuir* **2007**, *23*, 6677–6683.
(36) Patwardhan, S. V.; Maheshwari, R.; Mukherjee, N.; Kiick, K. L.; Clarson, S. J. *Biomacromolecules* **2006**, *7*, 491–497.
(37) Liu, Y.-L.; Chen, Y.-J. *Polymer* **2004**, *45*, 1797–1804.
(38) Kundu, D.; Zhou, H. S.; Honma, I. *J. Mater. Sci.* **1998**, *17*, 2089–2092.

AM9009378